Reaction Chemistry & Engineering

ROYAL SOCIETY OF CHEMISTRY

PAPER

View Article Online
View Journal | View Issue

Cite this: *React. Chem. Eng.*, 2024, **9**, 2740

Modular 3D printed flow system for efficient one-step synthesis of phenyl-functionalised silica-coated superparamagnetic iron oxide nanoparticles†

Andrea du Preez, [a] André M. Strydom, [b] Derek T. Ndinteh [a] and Elize Smit *[a]

Iron oxide nanoparticles (IONPs) are used in various applications, including magnetic solid phase extraction (MSPE), due to advantages such as excellent adsorption efficiency and easy separation from varied matrices using an external magnet. Here we introduce a low-cost 3D-printed modular flow system for the automated synthesis of phenyl-functionalised silica-coated iron oxide nanoparticles. This system consists of 3D-printed polypropylene (PP) reactors with varying geometries connected in series to synthesise bare IONPs, silica-coated IONPs, or phenyl-functionalised silica-coated IONPs using laminar flow regimes. The simplicity, affordability, robustness, and customisability of the system were illustrated. The synthesised IONPs were characterised using Fourier transform infrared (FTIR) spectroscopy, transmission electron microscopy (TEM), zeta potential, powder X-ray diffraction (XRD), thermogravimetric analysis (TGA) and vibrating sample magnetometry (VSM). The continuous flow system resulted in fast reactions under ambient conditions, with a production rate of approximately 5 mg min^{-1}. The produced IONPs were small (~10 nm), resulting in a larger surface-to-volume ratio. Furthermore, the synthesised IONPs retained large enough saturation magnetisation values, which together with larger surface-to-volume ratios, is ideal for MSPE.

Received 16th May 2024,
Accepted 1st August 2024

DOI: 10.1039/d4re00242c

rsc.li/reaction-engineering

Introduction

Magnetic solid-phase extraction (MSPE) is a solid-phase extraction (SPE) technique based on the use of magnetic sorbents.[1,2] These magnetic sorbents exhibit excellent adsorption efficiency and fast separation from the matrix by applying an external magnetic field.[3] Additional advantages include low solvent consumption, low toxicity, and low cost.[2]

Magnetic separation based on superparamagnetic iron oxide nanoparticles (IONPs) is convenient due to a cost-effective and straightforward synthetic process.[4,5] However, IONPs are prone to agglomeration and oxidation due to their high surface area and instability at a pH level of less than 4.0, negatively impacting their paramagnetic properties. A coating method to conjugate organic or inorganic materials onto the surface is usually applied to overcome this challenge.[6] Silica is a popular coating material for IONPs because of its porous structure, size-selective permeability, and chemical stability.[7] Additionally, it provides the possibility for further functionalisation[2,3,5] with, for example, a phenyl group.[8] Although not further explored here, it is important to mention that coating IONPs with silica makes them biocompatible, leading to many additional applications in biomedicine.[7]

Preparing IONPs is a multistep process, typically consisting of the synthesis of the IONPs, coating and/or stabilising the nanoparticles, followed by functionalisation. IONPs are often prepared using the co-precipitation method. This reaction has been performed in batch and flow, although the particle sizes and reaction times vary significantly (Table 1). Within the last decade or so, flow techniques for synthesising a variety of IONPs have been reported. Various flow regimes, including chaotic mixing,[9,10] droplet flow,[11–14] segmented flow[15] and laminar flow[16,17] have been used. Using fluidic devices improves chemical synthesis due to their small reaction volumes, which enhance heat and mass transfer rates, resulting in decreased reaction times.[18,19] In other words, IONPs can be synthesised in minutes using flow techniques compared to several hours for their batch counterparts.

[a] *Center for Natural Product Research, Department of Chemical Sciences, University of Johannesburg, Johannesburg, South Africa. E-mail: esmit@uj.ac.za*
[b] *Highly Correlated Matter Research Group, Department of Physics, University of Johannesburg, Auckland Park, South Africa*

† Electronic supplementary information (ESI) available. See DOI: https://doi.org/10.1039/d4re00242c

Table 1 Summary of IONPs synthesised using flow techniques

Year	IONP type	IONPs synthesis method	Stabilisation/coating method	Functionalisation method	Particle size (nm)	Reference
2009	Magnetic and fluorescent silica-coated γ-Fe_2O_3	Batch	Flow	Flow (separate reactor)	50	20
2012	Dextran-coated Fe_3O_4	Flow	Flow (same reactor)	N/A	3.6	11
2016	Oleic acid stabilised Fe_3O_4	Flow (spinning disc reactor)	Flow (same reactor)	N/A	2.9–9.3	21
2019	Linoleic acid-coated Fe_3O_4 and oleic acid-coated Fe_3O_4	Flow	Batch (sonication)	N/A	9–13	22
2020	Citric acid stabilised Fe_3O_4	Flow	Flow (separate reactor)	N/A	6–7	9
2021	Polyethylene glycol functionalised Fe_3O_4	Flow (base stabilised)	N/A	Flow (separate reactor)	7	23
2022	Bilayer oleic acid-coated Fe_3O_4 nanoclusters	Flow	Flow (separate reactor)	N/A	50–100[a]	24
2022	Aminopropyl silica-coated Fe_3O_4	Flow	Batch (sonication)	Batch (sonication, same vessel)	11–19	10
2022	Citric acid functionalised Fe_3O_4	Flow	N/A	Flow (same reactor)	4.3–4.6	25
2022	Carboxymethyl dextran coated Fe_3O_4	Flow	Flow (same reactor)	N/A	4–7	15
2023	Citric acid stabilised Fe_3O_4	Flow	Flow (separate reactor)	N/A	30	14

[a] Nanocluster size.

IONPs are mostly stabilised when using flow techniques by adding organic reagents such as citric acid,[9] linoleic acid,[22] palmitic acid,[22] and oleic acid[21] after synthesising the IONPs. The stabilising or coating agent is either added directly in flow or manually afterwards using a batch process. The Stöber method is one of the most common synthetic protocols for synthesising silica-coated IONPs. Generally, the IONPs are uniformly dispersed into an ethanol solution, followed by the addition of tetraethoxysilane (TEOS) and an aqueous solution of ammonia.[6] Similarly, the coated or stabilised IONPs can be functionalised in either batch or flow, however, depending on the intended application, functionalisation is not always necessary/reported. To the best of our knowledge, a continuous flow method using 3D-printed fluidic reactors for synthesising phenyl-functionalised silica-coated IONPs utilising a combination of the co-precipitation method and subsequent Stöber method has yet to be demonstrated.

This work aimed to develop an automated flow system for synthesising and coating IONPs. A flow method was selected based on the advantages already mentioned and the fact that a flow system is inherently automated. For the system to be effective and applicable, the following criteria must be met: simplicity, affordability, robustness, and customisability. Firstly, the system needs to be simple. The batch synthesis methods are relatively simple and must be replaced with a similarly simple flow method that does not require sophisticated equipment or experienced operators. Secondly, the system needs to be affordable and accessible. The prohibitive costs associated with commercial flow chemistry reactionware and equipment have led to the development of a wide variety of cost-effective alternatives fabricated using 3D printing.[26] Examples include open-source syringe pumps[27–29] and a wide variety of flow components[26,29–32] that are competitive with commercial counterparts. Thirdly, the system needs to be robust. By creating an automated system, nanoparticles can be synthesised repeatedly with the same physical and chemical characteristics. These parameters play a vital role in the final application of the synthesised materials, *e.g.*, in MSPE, the particle size will influence its surface-area-to-volume ratio, which will directly impact the extraction efficiency. At the same time, the magnetic properties will affect the ease of separating the nanoparticles from the sample matrix. Lastly, the system must be customisable. By designing a modular system, the end user will be free to fine-tune material properties and (degree of) functionalisation, by utilising different combinations of flow devices.

Method

Chemicals and materials

Iron(II) chloride tetrahydrate ($FeCl_2{\cdot}4H_2O$, 98%), iron(III) chloride hexahydrate ($FeCl_3{\cdot}6H_2O$, ≥98%), tetraethyl orthosilicate (TEOS, $C_8H_{20}O_4Si$, 98%), triethoxyphenylsilane (TEPS, $C_{12}H_{20}O_3Si$, 98%), and carbon film supported copper hexagonal mesh grids (grid size 200 mesh) were purchased from Merck. A 25% ammonium hydroxide (NH_4OH) solution and methanol (CH_4O, 99.5%) were purchased from Glassworld and Rochelle Chemicals, respectively. Furthermore, propan-2-ol (C_3H_8O, 99.7%) was purchased from UnivAR. Supelco tetrafluoroethylene (TFE) tubing (1.58 mm OD × 0.8 mm ID and 3.18 mm OD × 2.1 mm ID) was purchased from Merck. RS PRO clear polypropylene (PP) filament (general-purpose low-density PP, Catalog number: 174-0056, **https://za.rs-online.com/web/p/3d-printing-materials/1740056?gb=s**) with a diameter of 1.75 mm and neodymium magnets (25 mm × 10 mm) were purchased from

RS Components. All chemicals, reagents, and materials were used as received. Water was deionised before use.

Fluidic device channel geometry

Three fluidic reactors with different channel geometries were designed using Fusion 360 (Fig. 1). Devices with cylindrical channels (1 mm diameter) were considered and tested during preliminary experiments (details are provided in the ESI,† Fig. S1 and S2). After optimisation, the perpendicular channel T-reactor (Fig. 1B) was designed to have cylindrical channels. However, the first inlet channel and reaction zone had a diameter of 2 mm, whereas the second inlet channel had a diameter of 1 mm. The Y-reactor (Fig. 1C) was designed to have two cubic (1 mm × 1 mm) inlet channels that merge into a broader cuboid-shaped channel (1 mm × 2 mm) for the reaction zone.

All three fluidic reactors were designed with three access ports dedicated to two initial inlets and a single outlet. Furthermore, the reaction zone was designed to have a length of 30 mm and a height of 4 mm. A 4 mm high reaction zone results in transparent channels, which enables visual monitoring when clear 3D-printing filament is used as fabrication material. All access ports were designed to be compatible with commercial flangeless nuts with a 1/4″-28 UNF type threading. The total volumes of the designed fluidic reactors were estimated to be approximately 0.06 mL, 0.17 mL, and 0.09 mL for the head-on T-reactor (Fig. 1A), the perpendicular channel T-reactor (Fig. 1B), and the Y-reactor (Fig. 1C), respectively. Detailed images and dimensions are provided in Fig. S3–S5.†

Fabrication of flow system components

Fused deposition modelling (FDM) was used to fabricate all designed flow components and connections. This fabrication technique focuses on extruding semi-molten thermoplastic filament through a heated nozzle where each layer is printed individually until the completed three-dimensional object is obtained.[33,34] FDM is considered one of the most cost-effective 3D printing techniques due to the low cost of both the printer and its materials.[35] All flow components and connections were fabricated using transparent PP filament. Furthermore, transparent filament was used to visually monitor flow regimes, bubbles, and clog formation within the channels. PP is the preferred fabrication material for flow components and connections due to its thermostability up to 150 °C and chemical resistivity in a wide variety of solvents and chemicals.[33,36] The only disadvantage of using PP filament is that it is challenging to 3D-print. Some common challenges include poor bed adhesion and warping.[36] To consistently produce high-quality devices, it is important to store the filament in a resealable plastic bag or container while not in use, to avoid absorption of moisture.

In general, all objects were first designed using the computer aided design program (CAD), Fusion 360. The designed object was exported into a standard tessellation language (STL) file (see ESI†), which was then subsequently imported into a slicing program (PrusaSlicer, version 2.4.0) to set printing conditions and convert the STL file to a computer numerical control (CNC) programming language, *i.e.* G-code, for printing.

A Prusa i3 MK3S+ 3D printer was used to fabricate all fluidic reactors. Optimised printing conditions for PP fluidic devices were similar to previously reported work.[26] The flow devices were printed using a nozzle and bed temperature of 240 °C and 80 °C, respectively. When room temperatures were below 25 °C, higher printer bed temperatures were required (95–100 °C) to obtain leak-tight devices and avoid warping. A 0.4 mm nozzle and a layer height of 0.15 mm was used. All devices were printed on top of a layer of packing tape to improve bed adhesion. No support structures were required except for a 10 mm brim to minimise warping and increase bed adhesion. An infill of 100% and an extruder flow of 105% ensured leak-proof reactors with the necessary tightness of reactor channels, respectively.[36] The extruder flow was changed by editing the G-code (see ESI†). A rectilinear fill pattern was used with 5 solid layers (top and bottom). Perimeters were also set to be 5 layers thick. The minimum and maximum fan speeds were 35% and 100%, respectively. Default printing speeds were used (Table S1†).

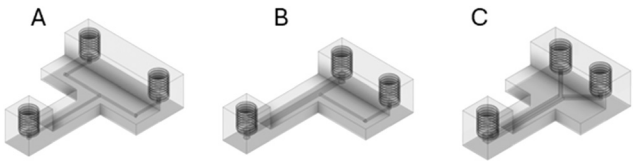

Fig. 1 The design of fluidic reactors with different geometries. (A) Head-on T-reactor with 1 mm channel diameters. (B) the perpendicular channel T-reactor consists of two inlet channels with 2 mm and 1 mm diameters that merge into a reaction zone with a 2 mm channel diameter. (C) Y-reactor with cubic (1 mm × 1 mm) and cuboid-shaped channels (1 mm × 2 mm) for the incoming reagent streams and reaction zone, respectively.

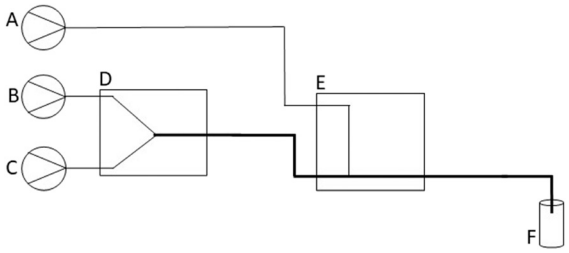

Fig. 2 Schematic diagram of the flow system used to synthesise phenyl-functionalised silica-coated IONPs at ambient temperature. (A) TEPS and TEOS solution. (B) Ammonia solution. (C) Iron ion precursor solution. (D) Y-reactor. (E) Perpendicular channel T-reactor. (F) Sample collection vial. All incoming reagent streams (A–C) had tubing with an I.D. of 0.8 mm, whereas the outlets of devices D and E and the subsequent first inlet of device E had tubing with an I.D. of 2.1 mm.

3D-printed flow system setup and operation

The 3D-printed Poseidon syringe pump set[28] was used for fluid delivery for the flow system. The configuration of the optimised modular flow system is depicted in Fig. 2. The flow system is modular because it consists of separate fluidic devices that can be joined together in different configurations to produce specific material (Fig. S7†). Solvent was allowed to flow through the system to determine the chemical compatibility of the reagents and flow components (including the 3D printed devices). No significant impurities or contaminants were observed (see ESI†).

To synthesise phenyl-functionalised silica coated IONPs, the flow system consisted of a Y-reactor (Fig. 2D) and a perpendicular channel T-reactor (Fig. 2E) placed in series. The Y-reactor (Fig. 2D) was used to synthesise BIONPs, whereas the perpendicular channel T-reactor (Fig. 2E) was used to simultaneously perform the coating and functionalisation steps. Incoming reagent streams (Fig. 2A–C) were connected to the reactor with TFE tubing with an inner diameter (I.D.) of 0.8 mm. However, the outlet of the Y-reactor and subsequent first inlet and outlet of the perpendicular channel T-reactor were connected with tubing with an I.D of 2.1 mm. This increase in tubing size is represented by the thicker line in Fig. 2.

The bare IONPs (BIONPs) were prepared using the flow configuration in Fig. S7(a)† and based on the co-precipitation method.[10] This flow method was adapted from a batch protocol reported by Benrabha and Tay[37] in 2019. An iron ion precursor solution was prepared by combining equal amounts of a 0.4 M $FeCl_2{\cdot}4H_2O$ solution and a 0.6 M $FeCl_3{\cdot}6H_2O$ solution. An iron solution with a ratio of 2 : 3 for Fe^{2+} to Fe^{3+} was selected since it enables the synthesis of magnetite (Fe_3O_4) in air atmosphere at ambient temperature.[37] The prepared iron ion precursor solution (Fig. 2C) was combined with a 7.5% ammonia solution (Fig. 2B) in a 3D-printed PP Y-reactor (Fig. 2D) at flow rates of 12 mL h^{-1} each. The BIONPs could be collected and isolated at this point.

Alternatively, the effluent from the first reactor, containing the synthesised BIONPs, could be introduced into the second reactor (*i.e.*, the perpendicular channel T-reactor). The solution containing a mixture of TEPS and TEOS (Fig. 2A) was introduced into this reactor at a flow rate of 15 mL h^{-1} (Fig. 2E). The TEPS percentage varied from 5.0% to 50.0% (Table 2), where the total volume of TEPS and TEOS remained 2 mL throughout. This TEPS and TEOS mixture was added to a solution of 50 mL propan-2-ol and 4 mL deionised water. The synthesised IONPs, *i.e.*, silica-coated (SIONPs) and phenyl-functionalised silica-coated (PSIONPs), were collected in a vial (Fig. 2F) and washed several times with deionised water and methanol using an external magnetic field. Before being introduced to the flow system, all reagent solutions were degassed by sonication at room temperature for 30 minutes, followed by manual degassing using a syringe and a piece of parafilm. Samples were freeze-dried prior to characterisation.

Table 2 Summary of the parameters for synthesising phenyl-functionalised silica-coated IONPs. The percentage of the volumes of TEPS in TEOS varied throughout. The total volume of the TEPS and TEOS mixture was 2 mL

Volume TEPS (mL)	Volume TEOS (mL)	Percentage TEPS (%)
0.00	2.00	0.0
0.10	1.90	5.0
0.22	1.78	11.0
0.67	1.33	33.5
0.89	1.11	44.5
1.00	1.00	50.0

Characterisation

The functional groups of BIONPs, SIONPs, and PSIONPs (synthesised with different percentages of TEPS in TEOS solutions) were identified using a Shimadzu IRSpirit Fourier transform infrared spectrometer with a scanning range of 400 to 4000 cm^{-1}, and a spectral resolution of 4 cm^{-1} in transmittance mode. The morphology, nanoparticle size distribution, and elemental composition of BIONPs, SIONPs, and PSIONPs were measured using a JOEL JEM-2100 transmission electron microscope (TEM) equipped with energy dispersion spectroscopy (EDS). The instrument operated at an accelerating voltage of 200 kV. Samples were prepared by sonicating approximately 10 mg of freeze-dried samples in 8 mL methanol for one hour. One drop of the prepared sample was placed on a carbon film supported by a copper hexagonal mesh grid. These grids were left to dry before imaging under the electron microscope. The average nanoparticle size and distribution were determined for all samples by manual image analysis using ImageJ.[16] Values were obtained by measuring at most N = 200 nanoparticles and were reported as D = nanoparticle diameter ± standard deviation (SD) in nm. Nanoparticle surface charges were determined by zeta potential measurements of the synthesised IONPs by dynamic light scattering (DLS) using a Malvern Zetasizer Nano ZS instrument. Approximately 20 mg of the sample was added to 100 mL of deionised water and sonicated for 30 minutes. All measurements were performed at ambient temperature at different pH levels. The pH adjustments were done using 0.1 M and 0.01 M potassium hydroxide (KOH) and hydrochloric acid (HCl) solutions. The sample was transferred into a disposable cuvette (fitted with a dip cell for zeta potential analysis) and measured in triplicate at 25 °C. The crystalline phases of the synthesised IONPs were determined by powder X-ray diffraction (pXRD) using a PANalytical Empyrean X-ray diffractometer equipped with Cu-Kα radiation (λ = 0.1542 Å) operating at 40 kV and 40 mA, with 2θ ranging from approximately 3° to 90°, step size of 0.013° and scan step time of 66.04 s. Thermal analysis was performed using a thermogravimetric analyser (TGA, SDT-Q600) with a heating rate of 10 °C min^{-1} from ambient temperature to 990 °C. The magnetic properties of the

synthesised magnetic nanoparticles were investigated using the vibrating sample magnetometer (VSM) platform of a DynaCool instrument (Quantum Design, San Diego) at fixed ambient temperature (300 K), and in applied magnetic fields between −20 000 Oe and +20 000 Oe. When sweeping the field from one datum point to the next, the field was stabilised at each desired field value before the magnetic moment was measured.

Results and discussions

Fluidic device performance

Three fluidic devices with varying channel geometries were initially used to synthesise BIONPs (Fig. S1 and S2†). During these experiments, it became apparent that the geometry, size, and shape of channels have a significant impact on the flow reaction. Other studies have not considered these details since typically only one device geometry is presented, especially when commercial T-mixers[9] and Y-mixers were used[10,38] that facilitate chaotic mixing regimes, since the mixer inlets and outlet are of the same diameter. Devices that facilitate mixing by diffusion *via* laminar flow regimes require specialised reactor types.[16,17,20,39] Therefore, the development of customised fluidic devices are justified since the junction between incoming streams and the dimensions of the reaction zone could be fine-tuned for optimal performance. The method development is described here to support the selection of reactors with specific geometries for the final flow system and provide insight into the challenges that may arise in other similar flow systems.

Initially, all devices had cylindrical channels with 1 mm diameters. Since all channels were the same size, chaotic mixing occurred in all devices regardless of channel geometry (Fig. S1†). These devices were prone to fouling within a few minutes, irrespective of the flow rate (6, 9, and 12 mL h^{-1}). Device fouling (*i.e.*, leaking) was often observed primarily at the access ports. Frequently tapping of the devices was required during the reaction to minimise fouling, which ultimately affects the automation of the flow reaction by increasing manual intervention. Furthermore, during reactions, it was observed that the black precipitate started to push backward into the incoming reagent streams. This observation indicated backpressure build-up due to a clog forming in the channel, possibly due to clogging by aggregation. Clogging by aggregation[40] occurs because bare iron oxide nanoparticles agglomerate due to van der Waals forces[5] within close distances[40] to one another.

Devices that facilitate laminar flow regimes and, hence, mixing by diffusion were considered to minimise fouling and tapping of devices during reactions. Therefore, a Y-reactor with cubic-shaped (1 mm × 1 mm) channels for incoming reagent streams that merge into a cuboid-shaped (1 mm × 2 mm) reaction zone was designed and fabricated (Fig. 1C and 2D). Utilising square channels with equal heights, allowed the inlet channels to align properly with the reaction zone, which cannot be achieved with cylindrical channels. The perpendicular channel T-reactor was also modified to house a 2 mm diameter channel for the first inlet channel and subsequent reaction zone and outlet. However, the second inlet channel remained unchanged (Fig. 1B and 2E).

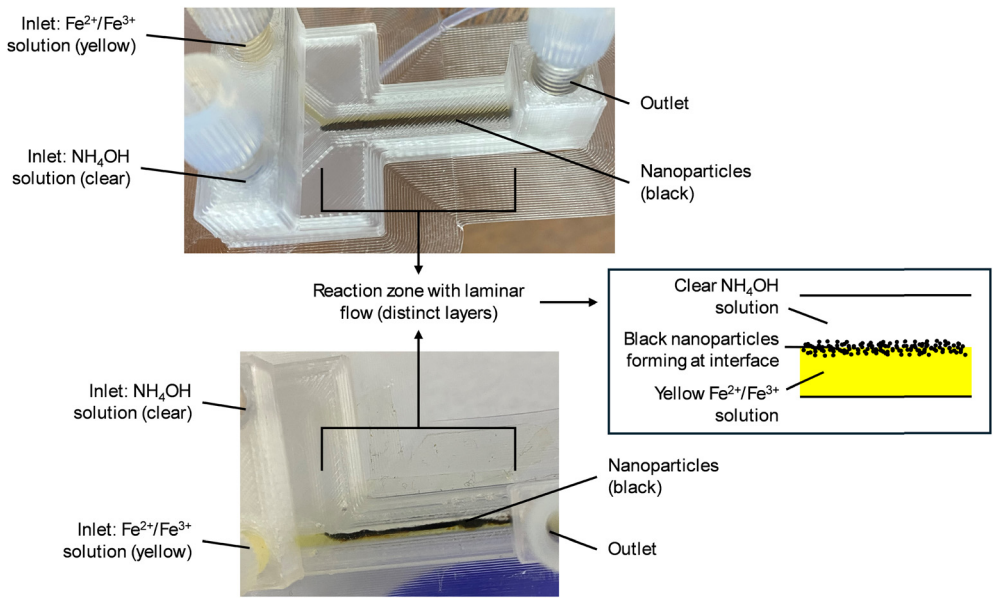

Fig. 3 3D-printed PP fluidic devices that facilitated laminar flow regimes when an iron ion precursor solution (yellow) mixes *via* diffusion with an ammonium hydroxide solution (clear) for the synthesis of bare IONPs (black solid). Top: Y-reactor (12 mL h^{-1} flow rate for the iron ion precursor and the ammonium hydroxide solution stream). Bottom: Perpendicular channel T-reactor (flow rates were 18 mL h^{-1} for the iron ion precursor solution stream and 9 mL h^{-1} for the ammonium hydroxide solution stream). Insert: illustration of different layers observed within the reaction zone.

Laminar flow regimes for both 3D-printed fluidic devices were observed, as shown in Fig. 3A and B. The Y-reactor performed better at faster flow rates (12 mL h^{-1} for both incoming reagent streams) compared to slower flow rates. Slower flow rates still required tapping to minimise fouling due to clogging by aggregation. However, at faster flow rates, any nanoparticle build-up in the reaction zone channel was discharged from the reaction zone by pressure from the incoming reagent streams. Furthermore, to prevent fouling of the perpendicular T-reactor, the flow rate for the iron ion precursor solution stream had to be faster compared to the ammonium hydroxide solution stream. This difference in flow rate resulted in an induced laminar flow regime, as seen in Fig. 3B. Since the Y-reactor with square channels performed better than all other designs, it was selected for the first step in the modular flow system to synthesise the BIONPs. The modified perpendicular T-reactor was chosen as the second device in the modular flow system for the coating and functionalisation steps since it performed well when the two incoming reagent streams differed in flow rate, which could be beneficial for the coating and functionalisation steps. Achieving laminar flow was crucial, since reagents are only in contact with each other at the interface between the two layers/streams, thereby allowing precise control of reaction rates and particle growth.

Flow system setup and operation

The 3D-printed modular flow system for synthesising PSIONPs was set up according to the diagram in Fig. 2 and shown in Fig. 4. Using a set of open-source Poseidon syringe pumps[28] and 3D-printed fluidic devices decreased the overall costs of the flow system. This flow method was considered safer than its batch counterpart since handling chemicals was limited. Additionally, a lower base-catalyst concentration of 7.5% was used compared to the 25% for its batch counterpart.[37] This was due to the characteristic improved reactivity of flow methodologies. Furthermore, since 3D printing is an effective and inexpensive fabrication technique, it was possible to increase throughput by 3D printing multiple fluidic reactors. With this methodology, PSIONPs can be synthesised within minutes, compared to approximately 24 hours using batch procedures.[8,37] The overall production rate was about 5 mg min^{-1} and reactions were carried out for approximately 35 minutes at a time. For the intended application of the material, *i.e.* MSPE, enough PSIONPs were produced during this time. If larger amounts of material are required, the authors would recommend scaling out the system rather than scaling up since the small channel sizes play an important role in synthesising small nanoparticles.

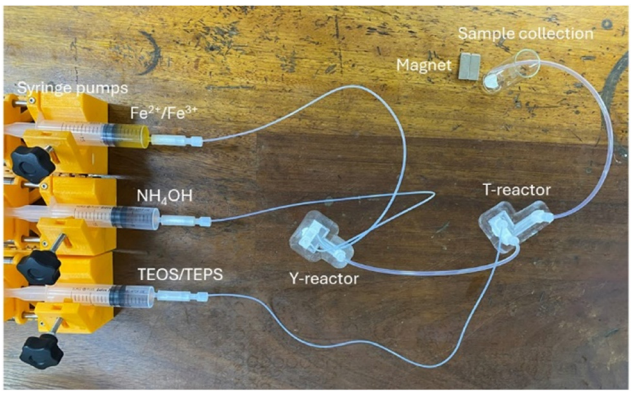

Fig. 4 The set-up of the 3D-printed modular flow system for synthesising PSIONPs. The flow system consisted of a set of Poseidon syringe pumps,[28] two 3D-printed fluidic reactors (Y-reactor and a T-reactor) connected in series, and a sample collection zone. The collected material was washed manually by applying an external magnetic field, prior to characterisation.

Characterisation of synthesised IONPs

The synthesised IONPs were fully characterised and detailed results and interpretations are provided in the ESI.† Briefly, the FT-IR spectrum for BIONPs (Fig. S8†) had characteristic absorption bands at 548 cm^{-1} and 3230 cm^{-1}, which corresponds to stretching and bending vibrations of Fe–O and H–O–H, respectively. An additional broad absorption band appeared at around 1058 cm^{-1} upon coating the surface with silica using TEOS to obtain SIONPs (Fig. S8†), which was due to the stretching vibrations of Si–O–Si in silica. The Fe–O absorption band at approximately 560 cm^{-1} persisted throughout the coating and functionalisation steps. The characteristic =C–H (sp^2) and C=C stretching bands for aromatic rings were observed at approximately 3053 cm^{-1} and 1430 cm^{-1}, respectively, for the PSIONPs at higher TEPS concentrations (33.5–50.0%). Zeta potential and EDS results are discussed in the ESI† and are shown in Fig. S10 and S11, respectively. The XRD patterns for all synthesised IONPs are shown in Fig. S12.† Characteristic diffraction peaks were present for the BIONPs. These diffraction peaks persisted in the XRD patterns for the coated and functionalised IONPs, which indicate that the crystalline phase of the IONPs was not significantly altered during the coating and functionalisation processes. Furthermore, a broad hump indicative of the presence of the amorphous silica shell was observed for the coated and functionalised IONPs. The TGA results are discussed in detail in the ESI† and shown in Fig. S13. A summary of the results from TEM, XRD, TGA, and VSM is provided in Table 3.

The TEM images obtained, and the resultant particle diameter distribution diagrams of all samples are shown in Fig. 5. The BIONPs had an estimated average particle diameter of 9.39 ± 1.17 nm (Fig. 5A) with a spherical to semi-spherical shape. The obtained average particle diameter was consistent with similar reported methods for the flow synthesis of BIONPs.[10,22] Coating the IONPs with silica, increased the average particle diameter to approximately 10.57 ± 1.77 nm (Fig. 5B). Furthermore, the SIONPs retained

Table 3 Summary of characterisation data of all samples synthesised in flow. Particle diameter (D) with standard deviations (SD) was determined manually using ImageJ software. The crystallite size diameters (d) with standard deviations (SD) were determined using the Scherrer equation. Magnetisation saturation (M_s) with relative standard deviation (RSD) is given

		TEM	XRD	TGA	Magnetism	
Entry	Sample	$D \pm$ SD (nm)	$d \pm$ SD (nm)	Total weight loss (%)	M_s (emu g^{-1}) ± RSD	M_r (emu g^{-1})
1	BIONPs	9.39 ± 1.17	9.16 ± 0.56	6.32	67.55 ± 0.0012	2.43
2	SIONPs	10.57 ± 1.77	8.64 ± 0.80	8.56	40.52 ± 0.0013	1.91
3	PSIONPs (5.0%)	11.10 ± 1.39	7.79 ± 1.20	11.5	41.89 ± 0.0056	1.55
4	PSIONPs (11.0%)	10.92 ± 1.30	8.47 ± 1.28	13.1	33.16 ± 0.0025	1.22
5	PSIONPs (33.5%)	11.35 ± 1.79	8.99 ± 1.32	20.1	29.92 ± 0.0018	1.24
6	PSIONPs (44.5%)	10.78 ± 1.42	8.99 ± 1.51	17.49	25.8 ± 0.0043	0.99
7	PSIONPs (50.0%)	11.24 ± 1.22	10.11 ± 1.73	21.41	38.61 ± 0.0011	1.58

its spherical to semi-spherical shape, however the particles were observed to be externally enclosed by a brighter matrix of TEOS, similar to what has been reported elsewhere.[10,41–43] The TEM images for the PSIONPs (Fig. 5C–G) appeared similar to that for the SIONPs (Fig. 5B), however the average particle diameters increased slightly with approximately 1 nm. From the distributions for the SIONPs (Fig. 5B) and the PSIONPs (Fig. 5C–G), the sizes of IONPs appear similar. This observation can be due to the constant total volume (2 mL) of TEOS and TEPS in solution (Table 2). Lastly, the reported batch synthesis by Rezvani *et al.*[44] and Benrabha *et al.*[37] of PSIONPs resulted in particles with diameters of approximately 50 nm. In comparison, the developed flow system presented here for the synthesis of these particles resulted in particles with an average diameter of approximately 11 nm at various TEPS in TEOS

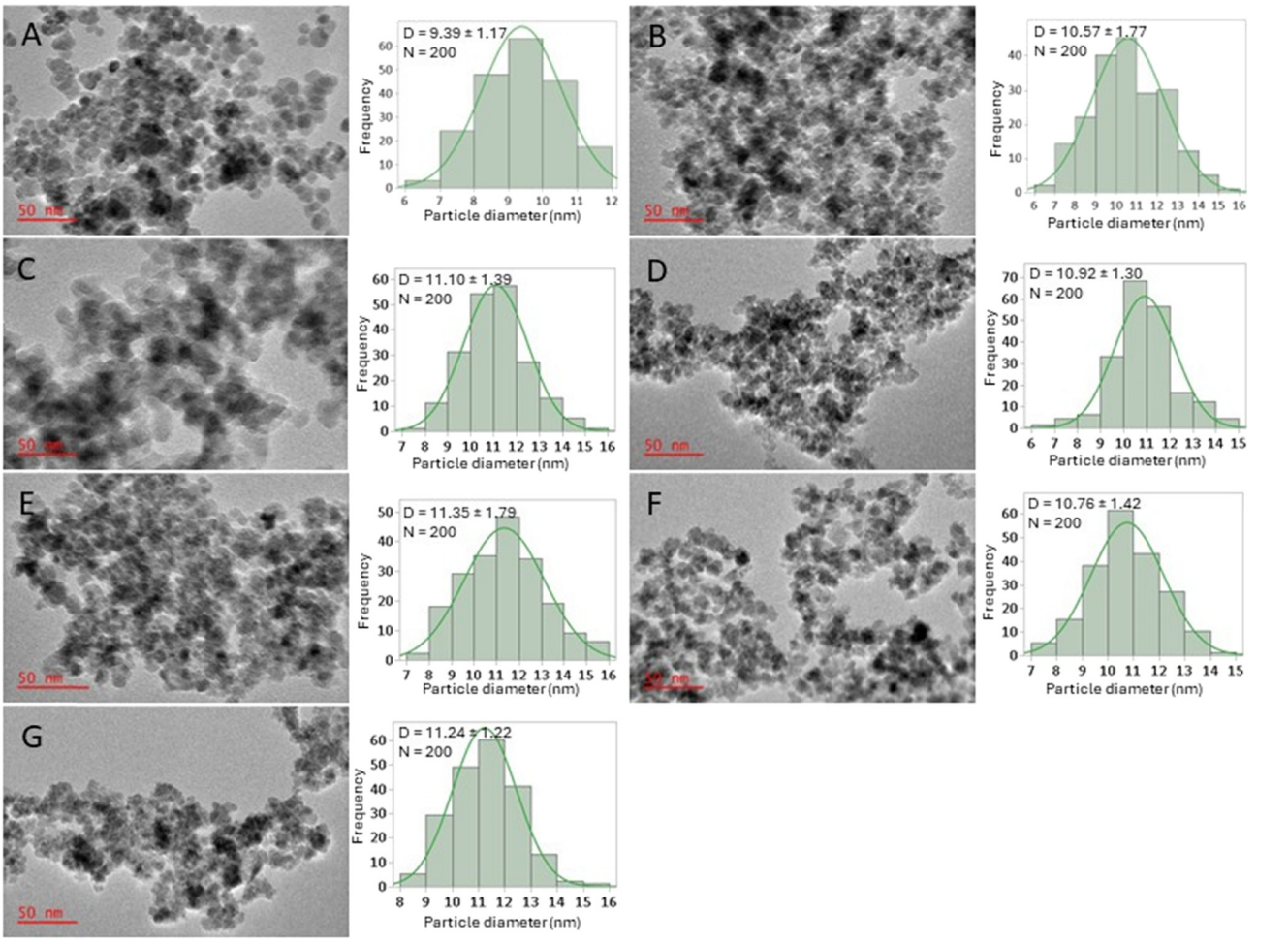

Fig. 5 TEM images at 50 nm magnification (left) and particle diameter distribution diagrams (right) of (A) BIONPs, (B) SIONPs, and PSIONPs with different percentages of TEPS in TEOS solutions (C) 5.0%, (D) 11%, (E) 33.5%, (F) 44.5%, (G) 50.0%.

concentrations. This observation is due to the small reaction channels typically used in flow that controls nanoparticle size,[17] especially under laminar flow conditions where reactions only take place at the interface of reagent layers.

The magnetic properties of the synthesised magnetic nanoparticles were investigated using the vibrating sample magnetometry (VSM) method at fixed ambient temperature (300 K), and in applied magnetic fields between −20 000 Oe and +20 000 Oe. Furthermore, magnetic parameters such as saturation magnetisation (M_s), and remnant magnetisation (M_r) were obtained from the magnetisation curves (Fig. 6) and are summarised in Table 3. For all synthesised magnetic IONPs, characteristic hysteresis loops with the typical S-shape were obtained (Fig. 6). The BIONPs had a M_s value of approximately 68 emu g^{-1} (Table 3, entry 1), which is comparable to reported values.[45–47] This M_s value is significantly less than that of bulk Fe_3O_4 (93 emu g^{-1}),[22] however, smaller particle sizes typically result in lower saturation magnetisation values.[46] For bulk ferromagnetic substances, the mean magnetic field is built up by neighbouring spins in the lattice structure of the material. However, for particles, surface effects can cause different spin-ordering, which in turn results in the reduction of the magnetic moment.[48]

Upon coating the BIONPs with silica using TEOS, the M_s value was drastically reduced to approximately 41 emu g^{-1} (Table 3, entry 2). This reduction in M_s is due to the presence of the surrounding diamagnetic SiO_2 shell[49,50] that has weakened the magnetic moment of the inner core and lessened the inductive effect of the magnetic field.[46] Furthermore, the obtained M_s value for SIONPs is comparable to reported values.[51–53] Initially, upon functionalisation with phenyl group using TEPS, a slight increase in M_s of approximately 1.4 emu g^{-1} was observed using a solution containing 5.0% TEPS (Table 3, entry 3). This slight increase in M_s indicates a slight decrease in the silica coating with few, if any, phenyl groups on the silica surface, which is consistent with the FT-IR results. When the percentages of TEPS ranged between 11.0% and 44.5%, further reduction of M_s values were observed, except for when the TEPS percentage was 50.0% (Table 3, entry 7). However, all M_s values were lower compared to that of SIONPs (Table 3, entry 2). This shows that in the coating process, when the percentages of TEPS increased, so did the layer formation consisting of silica and phenyl-functionalised silica, which resulted in a decrease of M_s. In the case of the 50.0% TEPS (Table 3, entry 7), the increase in M_s could be due to a reduction of the formation of the silica coating as well as a thinner phenyl-silica layer. Similar observations were made by Mokkarat *et al.*[10] in the case of the flow synthesis of aminopropyl-functionalised SIONPs. Additionally, this observation is also consistent with the XRD results (Fig. S12†). Most importantly, the SIONPs, as well as all the PSIONPs, have large enough M_s values to facilitate magnetic separation using an external magnet for MSPE applications. Lastly, the M_r values (Table 3) are relatively close to zero for all synthesised IONPs. Thus, the synthesised IONPs are all considered superparamagnetic and comparable to literature.[46]

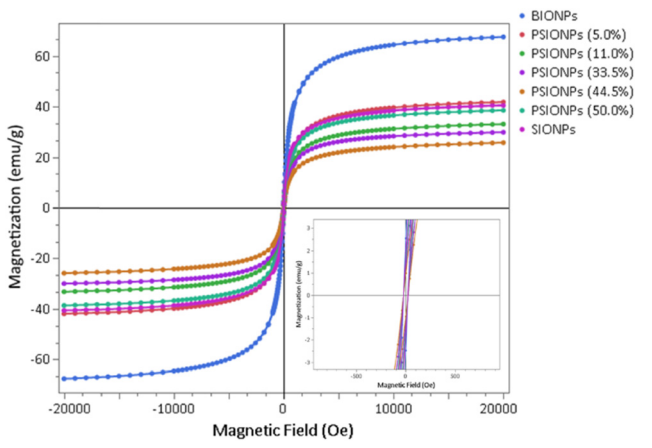

Fig. 6 VSM magnetisation curves of the magnetic nanoparticles synthesised in flow using 3D-printed devices. The insert shows the behaviour of the magnetisation at very small fields.

Conclusions

A 3D-printed modular flow system was developed for the one-step synthesis of PSIONPs for MSPE purposes. This flow system is convenient and straightforward to use since one reactor facilitates the synthesis of BIONPs, and a second reactor can be applied for the simultaneous coating and functionalisation of the nanoparticles. Note that coating and functionalisation can be achieved in a single step. Higher percentages of TEPS (in TEOS) were preferred for preparing functionalised PSIONPs. The functionalised magnetic nanoparticles were much smaller than their batch counterparts due to small reaction channels. Even though saturation magnetisation was lower than what has been reported for bulk Fe_3O_4, it was still sufficiently large enough to facilitate separation from solution with an external magnetic field. Furthermore, the functionalised magnetic nanoparticles retained their magnetic properties, which is essential for MSPE applications. The four basic criteria: simplicity, affordability, robustness, and customisability were met. Firstly, because the flow system is simple to assemble, operate and required no sophisticated equipment. Secondly, since 3D-printing and open-source hardware were used, costs were kept as low as possible. Thirdly, the flow system was robust, since IONPs with similar physical and chemical characteristics could be synthesised repeatedly. Lastly, the flow system is customisable since the modular approach allows for synthesis of BIONPs, SIONPs, and PSIONPs as desired, while reaction parameters (*e.g.* % TEPS) can be fine-tuned to achieve the desired degree of functionalisation. Furthermore, this flow system can be adapted for the synthesis of a wide variety of iron oxide nanoparticles for numerous applications.

Data availability

The data supporting this article, together with the STL files for all 3D-printed reactors, have been included as part of the ESI.†

Author contributions

AdP: conceptualisation, formal analysis, investigation, methodology, visualisation, writing – original draft, writing – review & editing. AMS: formal analysis, investigation, resources, writing – review & editing. DTN: conceptualisation, supervision, writing – review & editing. ES: conceptualisation, funding acquisition, resources, supervision, visualisation, writing – original draft, writing – review & editing.

Conflicts of interest

The authors declare no competing financial interest.

Acknowledgements

The authors would like to thank Sindi Xhakaza, for assistance with VSM measurements. AMS thanks the URC/FRC of UJ and the NEP programme of the SA-NRF (105702) for financial assistance. AdP thanks the UJ GES programme for a scholarship. ES thanks SA-NRF (138415) for financial assistance.

Notes and references

1 C. C. Acebal, B. M. Simonet and M. Valcárcel, *TrAC, Trends Anal. Chem.*, 2013, **43**, 109–120.
2 M.-M. Zhao, H.-Z. Wu, X.-K. Deng, R.-N. Yi and Y. Yang, *Anal. Methods*, 2024, **16**, 333–343.
3 M. Hemmati, M. Rajabi and A. Asghari, *Microchim. Acta*, 2018, **185**, 160.
4 R. Keçili, F. Ghorbani-Bidkorbeh, İ. Dolak, G. Canpolat, M. Karabörk and C. M. Hussain, *TrAC, Trends Anal. Chem.*, 2021, **143**, 116380.
5 S. Natarajan, K. Harini, G. P. Gajula, B. Sarmento, M. T. Neves-Petersen and V. Thiagarajan, *BMC Med.*, 2019, **1**, 1–22.
6 N. Zhu, H. Ji, P. Yu, J. Niu, M. U. Farooq, M. W. Akram, I. O. Udego, H. Li and X. Niu, *Nanomaterials*, 2018, **8**, 1–27.
7 Y. J. Wong, L. Zhu, W. S. Teo, Y. W. Tan, Y. Yang, C. Wang and H. Chen, *J. Am. Chem. Soc.*, 2011, **133**, 11422–11425.
8 M. Saraji and N. Khaje, *J. Sep. Sci.*, 2013, **36**, 1090–1096.
9 M. O. Besenhard, A. P. LaGrow, A. Hodzic, M. Kriechbaum, L. Panariello, G. Bais, K. Loizou, S. Damilos, M. Margarida Cruz, N. T. K. Thanh and A. Gavriilidis, *Chem. Eng. J.*, 2020, **399**, 125740.
10 A. Mokkarat, S. Kruanetr and U. Sakee, *J. Saudi Chem. Soc.*, 2022, **26**, 101506.
11 K. Kumar, A. M. Nightingale, S. H. Krishnadasan, N. Kamaly, M. Wylenzinska-Arridge, K. Zeissler, W. R. Branford, E. Ware, A. J. Demello and J. C. Demello, *J. Mater. Chem.*, 2012, **22**, 4704–4708.
12 L. Frenz, A. El Harrak, M. Pauly, S. Bégin-Colin, A. D. Griffiths and J. C. Baret, *Angew. Chem., Int. Ed.*, 2008, **47**, 6817–6820.
13 V. Singh, *J. Flow Chem.*, 2021, **11**, 135–142.
14 M. O. Besenhard, S. Pal, L. Storozhuk, S. Dawes, N. T. K. Thanh, L. Norfolk, S. Staniland and A. Gavriilidis, *Lab Chip*, 2023, **23**, 115–124.
15 J. Schemberg, A. El Abbassi, A. Lindenbauer, L. Chen, A. Grodrian, X. Nakos, G. Apte, N. Khan, A. Kraupner, T.-H. Nguyen and G. Gastrock, *ACS Appl. Mater. Interfaces*, 2022, **14**, 48011–48028.
16 M. Simmons, C. Wiles, V. Rocher, M. G. Francesconi and P. Watts, *J. Flow Chem.*, 2013, **3**, 7–10.
17 A. Abou Hassan, O. Sandre, V. Cabuil and P. Tabeling, *Chem. Commun.*, 2008, 1783–1785.
18 K. Amreen and S. Goel, *ECS J. Solid State Sci. Technol.*, 2021, **10**, 017002.
19 M. B. Kulkarni and S. Goel, *Nano Express*, 2020, **1**, 032004.
20 A. Abou-Hassan, R. Bazzi and V. Cabuil, *Angew. Chem., Int. Ed.*, 2009, **48**, 7180–7183.
21 F. Haseidl, B. Müller and O. Hinrichsen, *Chem. Eng. Technol.*, 2016, **39**, 2051–2058.
22 R. Sawisai, R. Wanchanthuek, W. Radchatawedchakoon and U. Sakee, *Surf. Interfaces*, 2019, **17**, 100344.
23 J. Mahin, C. O. Franck, L. Fanslau, H. K. Patra, M. D. Mantle, L. Fruk and L. Torrente-Murciano, *React. Chem. Eng.*, 2021, **6**, 1961–1973.
24 L. Zhou, L. Ye and Y. Lu, *Nanomaterials*, 2022, **12**, 350.
25 N. Akkurt, C. L. Altan and M. F. Sarac, *J. Supercond. Novel Magn.*, 2022, **35**, 615–623.
26 A. du Preez, R. Meijboom and E. Smit, *Food Anal. Methods*, 2022, **15**, 1816–1825.
27 B. Wijnen, E. J. Hunt, G. C. Anzalone and J. M. Pearce, *PLoS One*, 2014, **9**, e107216.
28 A. S. Booeshaghi, E. D. V. Beltrame, D. Bannon, J. Gehring and L. Pachter, *Sci. Rep.*, 2019, **9**, 12385.
29 J. M. Neumaier, A. Madani, T. Klein and T. Ziegler, *Beilstein J. Org. Chem.*, 2019, **15**, 558–566.
30 A. J. N. Price, A. J. Capel, R. J. Lee, P. Pradel and S. D. R. Christie, *J. Flow Chem.*, 2021, **11**, 37–51.
31 P. J. Kitson, S. Glatzel and L. Cronin, *Beilstein J. Org. Chem.*, 2016, **12**, 2776–2783.
32 G. W. Bishop, J. E. Satterwhite, S. Bhakta, K. Kadimisetty, K. M. Gillette, E. Chen and J. F. Rusling, *Anal. Chem.*, 2015, **87**, 5437–5443.
33 V. Dragone, V. Sans, M. H. Rosnes, P. J. Kitson and L. Cronin, *Beilstein J. Org. Chem.*, 2013, **9**, 951–959.
34 T. Tabassum, M. Iloska, D. Scuereb, N. Taira, C. Jin, V. Zaitsev, F. Afshar and T. Kim, *J. Chem. Educ.*, 2018, **95**, 783–790.
35 V. Romanov, R. Samuel, M. Chaharlang, A. R. Jafek, A. Frost and B. K. Gale, *Anal. Chem.*, 2018, **90**, 10450–10456.
36 Z. X. Rao, B. Patel, A. Monaco, Z. J. Cao, M. Barniol-Xicota, E. Pichon, M. Ladlow and S. T. Hilton, *Eur. J. Org. Chem.*, 2017, **2017**, 6499–6504.

37 A. M. Faraj Benrabha and K. S. Tay, *Green Process. Synth.*, 2019, **8**, 54–61.
38 M. Perissé Moreira and D. Grasseschi, *J. Nanopart. Res.*, 2022, **24**, 93.
39 G. Gkogkos, M. O. Besenhard, L. Storozhuk, N. T. K. Thanh and A. Gavriilidis, *Chem. Eng. Sci.*, 2022, **251**, 117481.
40 E. Dressaire and A. Sauret, *Soft Matter*, 2017, **13**, 37–48.
41 Z. Bednarikova, M. Kubovcikova, I. Antal, A. Antosova, M. Gancar, J. Kovac, R. Sobotova, V. Girman, D. Fedunova, M. Koneracka, Z. Gazova and V. Zavisova, *Surf. Interfaces*, 2023, **39**, 102942.
42 I. Al Kawni, R. Garcia, S. Youssef, M. Abboud, J. Podlecki and R. Habchi, *Mater. Res. Express*, 2016, **3**, 125024.
43 H. Lee, C. Kang, Y. Kuo and S. Tseng, *J. Food Drug Anal.*, 2021, **29**, 391–401.
44 O. Rezvani, M. H. Hedeshi and H. Bagheri, *Anal. Chim. Acta*, 2020, **1136**, 51–61.
45 J. Zou, Y. Peng and Y. Tang, *RSC Adv.*, 2014, **4**, 9693.
46 M. H. R. Farimani, N. Shahtahmasebi, M. Rezaee Roknabadi, N. Ghows and A. Kazemi, *Phys. E*, 2013, **53**, 207–216.
47 B. Zeynizadeh and M. Gilanizadeh, *Res. Chem. Intermed.*, 2020, **46**, 2969–2984.
48 M. O. Besenhard, L. Panariello, C. Kiefer, A. P. LaGrow, L. Storozhuk, F. Perton, S. Begin, D. Mertz, N. T. K. Thanh and A. Gavriilidis, *Nanoscale*, 2021, **13**, 8795–8805.
49 F. Chen, Y. Xiao, B. Zhang, R. Chang, D. Luo, L. Yang, Y. Yang and D. Liu, *J. Chromatogr. A*, 2020, **1613**, 460671.
50 S. A. A. Noma, A. Ulu, S. Koytepe and B. Ateş, *Biocatal. Biotransform.*, 2020, **38**, 392–404.
51 X. Zhao, Y. Shi, T. Wang, Y. Cai and G. Jiang, *J. Chromatogr. A*, 2008, **1188**, 140–147.
52 F. Alemi-Tameh, J. Safaei-Ghomi, M. Mahmoudi-Hashemi and R. Teymuri, *Res. Chem. Intermed.*, 2016, **42**, 6391–6406.
53 A. H. Gemeay, B. E. Keshta, R. G. El-Sharkawy and A. B. Zaki, *Environ. Sci. Pollut. Res.*, 2020, **27**, 32341–32358.